PART-B

Silicotungstates anchored to MCM-22

Chapter 1

Parent Silicotungstic acid (SiW_{12}) anchored to MCM-22:

Synthesis, Characterization and Esterification as well as Acetalization reactions

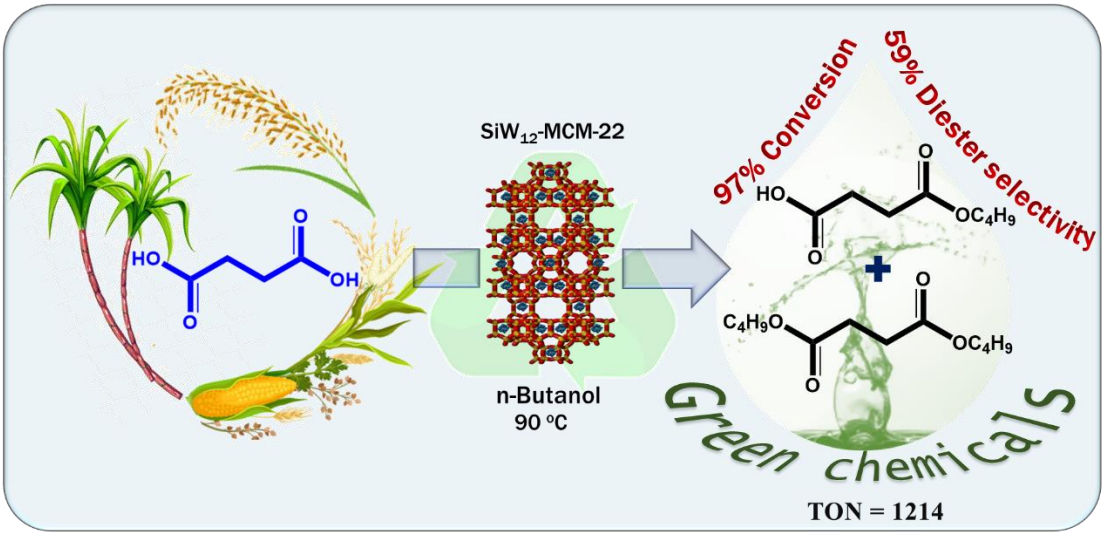

Biomass and Bioenergy 151 (2021) 106178

Contents lists available at ScienceDirect

Biomass and Bioenergy

journal homepage: www.elsevier.com/locate/biombioe

Conversion of bioplatform molecule, succinic acid to value-added products via esterification over 12-tungstosilicic acid anchored to MCM-22

Dhruvi Pithadia, Anjali Patel *

Polyoxometalates and Catalysis Laboratory, Department of Chemistry, Faculty of Science.,The Maharaja Sayajirao University of Baroda. Vadodara, 390002, Gujarat, India

ARTICLE INFO

Keywords:
Bioplatform molecule
Succinic acid
Diesterification
Heterogeneous catalyst
Anchored 12-tungstosilicic acid

ABSTRACT

The model bioplatform molecule succinic acid, via esterification with n-butanol, leads to succinate esters, promising fuel additives and value-added products. In the present article, the potential application of heterogeneous catalyst comprising silicotungstic acid (SiW_{12}) and MCM-22 (SiW_{12}-MCM-22) was exploited for esterification of succinic acid with n-butanol. Performance of the catalyst was examined by carrying out a detailed optimization study, focusing on the synthesis of diester (one of the excellent fuel additives) and kinetic experiments at different reaction time and temperatures. The experimental results exhibit synergistic effect of SiW_{12} and MCM-22, yielding 97% conversion of acid with 59% selectivity of diester, TON of 1214 and activation energy of 68 $kJmol^{-1}$. Experiments to demonstrates the effectiveness of High Gravity approach were also performed. The green metrics, atom economy (86.47%) (for desired diester) with E-factor (0.69) were calculated. The catalyst was recovered and used for consecutive three catalytic cycles, exhibiting remarkable regenerative activity to synthesize esters and contribute new routes for industrial scale.

In recent years, heterogeneous catalysis by zeolitic materials has gained tremendous attention predominantly in industrial processes. These microporous structures have been offering unique combination of properties for accessibility and transport of molecules inside the pores to effectively catalyse the desired transformations. Despite these assets, zeolites face diffusional constraints due to cavities and pores of nanometric magnitudes. In this direction, the concept of hierarchical zeolites such as Mobil Composite Material- 22 (MCM-22), which possess secondary porosity level with combination of improved pore size and inherent acidity have levelled up remarkably the conversion and catalytic rate of many industrial reactions [1–3].

In recent times, several fertile attempts have been reported for modification of MCM-22 by doping metals/metal oxides [4–11] and organic moieties [12]. Also, many potential industrial applications in several organic transformations for instance, oxidation [8,9,11], alkylation [13] and dehydration [14]. have been studied. However, only one report is available by Julian et al. [15], where POMs (polyoxomolybdate anions) were used as Mo precursors to modify MCM-22 for dehydroaromatization reaction. It is also important to note that till now, no efforts have been made to utilize this zeotype as a support for anchoring POMs particularly, silicotungstates and also for the catalytic transformation of the bioplatform molecules.

Thus, in the present chapter, a new catalyst comprising silicotungstic acid and zeolitic support, MCM-22 was synthesized by the wet impregnation method. Detailed characterization was carried out by acidity measurement, BET surface area measurements, elemental analysis (EDS), TGA, FT-IR, Powder XRD, ^{29}Si MAS NMR and TEM. The catalytic behaviour was investigated for the esterification as well as acetalization reaction of said bioplatform molecules and their detailed optimization study was carried out. The experiments in varying reaction parameters, such as mole ratio of reactants, catalyst amount, reaction temperature and time were screened and the optimum conditions were found,

where maximum conversion of a substrate and the desired product was achieved. The sustainable nature and reliability of the catalyst were checked by recycling experiments as well as characterization of regenerated catalyst. Kinetic experiments were carried out to determine the activation energy for all transformations. Moreover, a mechanism for each system was proposed.

EXPERIMENTAL

Materials

All the chemicals used were of A. R. grade. Silicotungstic acid, levulinic acid, succinic acid, glycerol, furfural, n-butanol, methanol, 2-propanol and dichloromethane were used as received from Merck. Zeolite MCM-22 was obtained commercially from BEE CHEMS (Kanpur, UP).

Synthesis of catalyst, silicotungstic acid anchored to MCM-22 (SiW_{12}/MCM-22)

Catalysts comprising SiW_{12} (10 - 40 %) anchored to MCM-22 were synthesized by the wet impregnation method. In an aqueous solution of SiW_{12} (0.1 g in 10 mL – 0.4 g in 40 mL of distilled water), 1 g of MCM-22 was added. The resulting suspension was dehydrated at 100 ˚C, followed by drying for 10 h. The obtained catalysts were designated as $(SiW_{12})_1$/MCM-22, $(SiW_{12})_2$/MCM-22, $(SiW_{12})_3$/MCM-22, and $(SiW_{12})_4$/MCM-22, respectively. A schematic representation of the procedure is shown in Scheme 1.

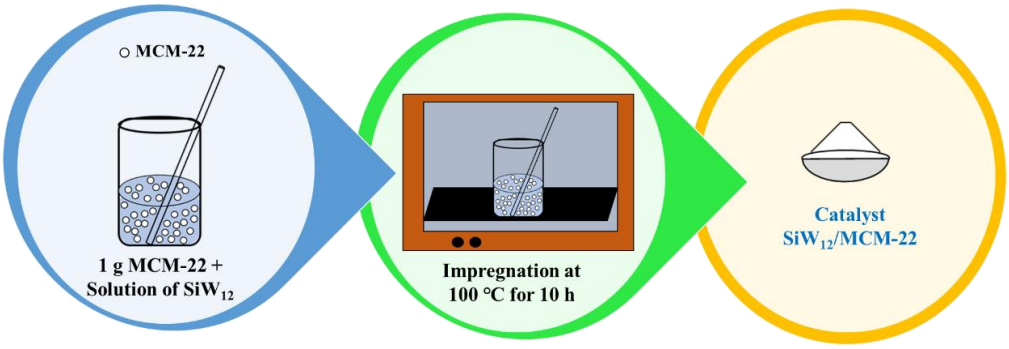

Scheme 1 Synthesis of SiW_{12}/MCM-22

Characterization

Characterization of SiW_{12}/MCM-22 was carried out by the same physicochemical techniques as mentioned in General Introduction [Page 41-46]

Catalytic activity

The esterification reaction of levulinic acid and succinic acid as well as the acetalization reaction of glycerol were carried out by following the same method as mentioned in General Introduction [Page 47-49].

RESULTS AND DISCUSSION

Characterization

Acidity measurement

Table 1 depicts the obtained results from the potentiometric titration of MCM-22 as well as all catalysts and the change in the electrode potential as a function of mEq/g of n-butylamine is shown in Figure 1. MCM-22 exhibits a reasonable acidic character having acidic strength of 132 mV and total sites of 1.4 mEq/g. Noted that even though, this support contains a silica-alumina framework, its acidity is less as compared to that of nMCM-48 (refer Table 1 in Part A Chapter 1). The initial electrode potential, also known as acidic strength, of MCM-22, increases with the impregnation of acidic species, SiW_{12}. Also, the acidic sites of the catalysts were found to increase from 10% to 30%, which bids the enriched distribution of SiW_{12} into the pores of the MCM-22. On the contrary, when the amount of SiW_{12} increased to 40%, the acidic strength and the sites remain almost the same. This unchanged behaviour may be attributed to the saturation of porous framework that may not uptake the excess keggin species. Henceforth, a 30% loading amount was found to be optimum.

Table 1 Acidity measurements of support and catalysts

Materials	Acidic strength (mV)	Types of acidic sites (mEq/g)		Total No. of acidic sites (mEq/g)
		Very strong	Strong	
MCM-22	132	0.2	1.2	1.4
$(SiW_{12})_1$/MCM-22	258	0.6	1.1	1.7
$(SiW_{12})_2$/MCM-22	382	1.4	1.0	2.4
$(SiW_{12})_3$/MCM-22	456	2.2	1.5	3.7
$(SiW_{12})_4$/MCM-22	482	2.1	1.8	3.9

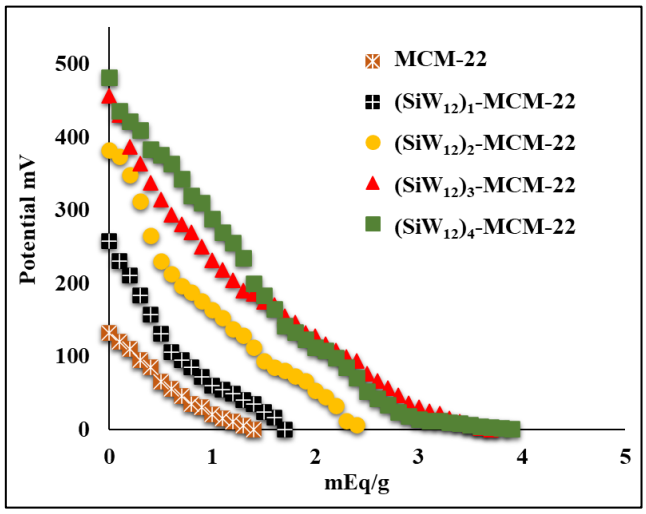

Figure 1 Potentiometric titration curves

BET surface area measurement

The BET surface area of MCM-22 and catalysts are mentioned in Table 2. As compared to MCM-22, the surface area, pore diameter and volume of catalysts obtained are lower, which is another indication of the incorporation of SiW_{12} species inside the zeolitic pores of MCM-22, after the acidity measurements. This trend is evident in 10 - 30% loaded catalysts. But, when the concentration increased to 40%, a little bit of increase in the pore diameter and volume was seen. Also, there was no significant change in surface area. This observation is well supported by acidity measurements. Hence here also we found 30%

loading of SiW_{12}, as an appropriate amount. From here, the detailed characterization of the 30% loaded catalyst was carried out and it is redesignated as SiW_{12}/MCM-22.

Table 2 Textural properties of support and catalysts

Materials	BET Surface area (m^2/g)	Pore diameter (Å)	Pore volume (cm^3/g)
MCM-22	344	102.4	0.79
$(SiW_{12})_1$/MCM-22	259	101	0.68
$(SiW_{12})_2$/MCM-22	243	94	0.60
$(SiW_{12})_3$/MCM-22	234	60.8	0.28
$(SiW_{12})_4$/MCM-22	230	61	0.50

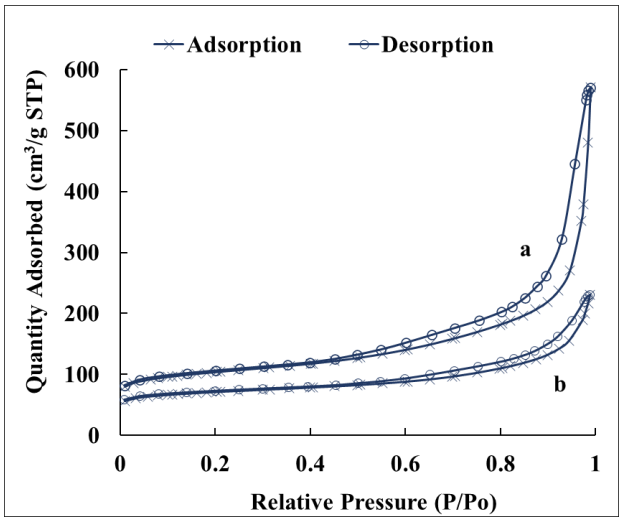

Figure 2 Nitrogen adsorption-desorption isotherms of a) MCM-22 and b) SiW_{12}/MCM-22

The Nitrogen adsorption-desorption isotherms of MCM-22 and SiW_{12}/MCM-22 are shown in Figure 2. MCM-22 exhibits type IV isotherm with H4 hysteresis loop, exhibiting a regular trend of zeolites, having micro as well as mesopores in the framework [16]. The adsorption starting at very low relative pressure, P/Po and extending up to higher value, forms a virtually horizontal plateau which is in good accord with the characteristic zeolitic nature of materials [17]. An identical isotherm was obtained for SiW_{12}/MCM-22, however, a

comparative narrow hysteresis loop was observed which corroborates the effective filling of SiW_{12} into the pores of MCM-22.

Elemental analysis

The elemental analysis was carried out for detecting the effective loading of SiW_{12} onto MCM-22. Figure 3 shows the presence of all expected elements while the value in Table 3, in terms of wt % of tungsten (W) for SiW_{12}/MCM-22, was in good agreement with the theoretically calculated value. Hence, it can be confirmed that the desired amount of SiW_{12} has been successfully impregnated onto the support.

Table 3 Elemental analysis of catalyst

Material	Si (wt%)	O (wt%)	Al (wt%)	W (wt%)	
				By EDS	Theoretical
SiW_{12}/MCM-22	19.43	53.86	9.38	17.33	17.7

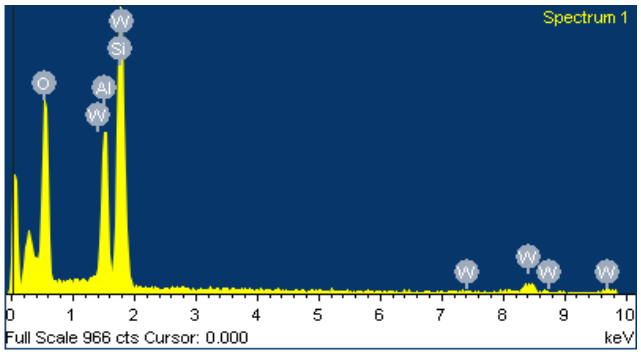

Figure 3 EDS elemental mapping of SiW_{12}/MCM-22

TGA

The TGA curves for MCM-22 and SiW_{12}/MCM-22 are shown in Figure 4. MCM-22 shows the weight loss in two steps. The initial weight loss of about 4.7% was observed up to 135 °C due to the desorption of physically adsorbed water molecules. The second weight loss of approximately 2.5% was seen above 200 °C which may be attributed to the decomposition of the template, which was not completely removed [18]. In the case of SiW_{12}/MCM-22, comparatively, a

higher weight loss (7.3%) was observed up to 144 °C, for the removal of adsorbed water molecules. Following that a gradual weight loss of 2.1% at 200 to 310 °C was obtained for the loss of crystalline water molecules present in the Keggin unit. After that, the weight loss of the catalyst was not observed which indicates its better thermal stability up to 500 °C.

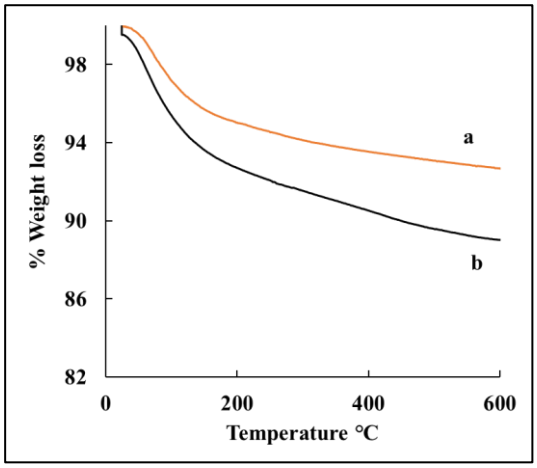

Figure 4 TGA curves of a) MCM-22 and b) SiW_{12}/nMCM-22

FT-IR

Figure 5 represents the FT-IR spectra of SiW_{12}, MCM-22 and SiW_{12}/MCM-22. MCM-22 exhibits characteristic bands at 3441 cm^{-1}, 1226 cm^{-1}, 817 cm^{-1} and 455 cm^{-1}. The band observed at 3441 cm^{-1} corresponds to the O-H stretching of a hydroxyl group of loosely bound water molecules. Bands at 817 cm^{-1} and 1226 cm^{-1}, can be attributed to the symmetric and asymmetric stretching vibrations of the T-O-T bond respectively, where T= Si or Al. A stretching vibration for T-O, where the metal ion is bonded to four oxygen atoms is observed at 455 cm^{-1} [19]. All the characteristic bands of MCM-22 are present in the FT-IR of SiW_{12}/MCM-22, suggesting the unchanged structure of support. An additional band appeared at 925 cm^{-1}, which is one of the characteristic bands for the Keggin unit of SiW_{12}, corresponding to asymmetric vibration of (Si-Oa). However, the other bands of SiW_{12} are not distinct due to their superimposition with the bands of MCM-22. Thus, the presence of this fingerprint band indicates that the primary of the Keggin unit is intact even after impregnation on the support.

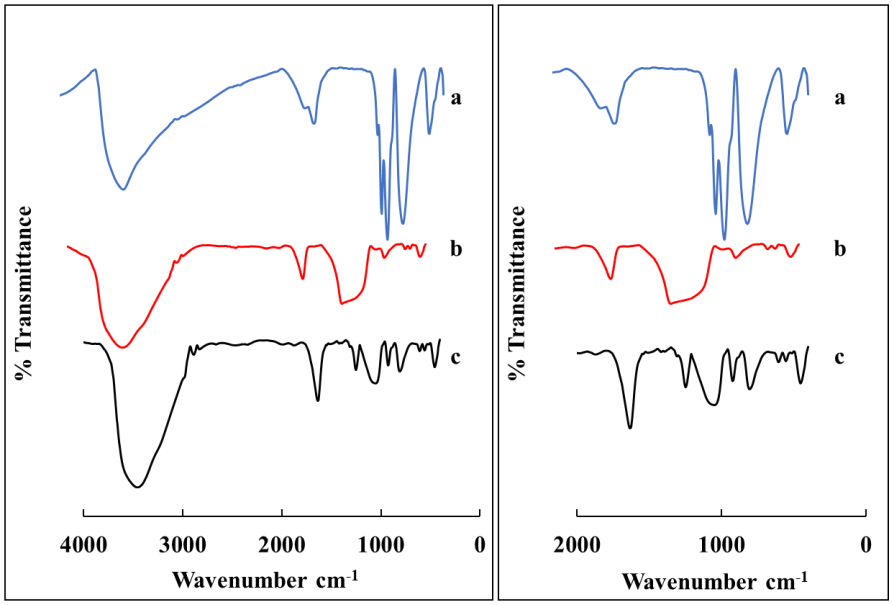

Figure 5 FT-IR spectra of a) SiW_{12}, b) MCM-22 and c) SiW_{12}/MCM-22

Powder XRD

The powder XRD patterns of SiW_{12}, MCM-22 and SiW_{12}/MCM-22 are illustrated in Figure 6. MCM-22 and SiW_{12}/MCM-22 show well-resolved characteristic patterns pertaining to the MWW framework, one of the forms of zeolitic structure, in the range of 2θ 5 - 30^{o} [20]. It recommends that the crystalline framework of MCM-22 remains unaffected even after the impregnation of SiW_{12}. But less intense peaks are observed for the catalyst which can be attributed to the inclusion of SiW_{12} inside MCM-22 and a minor loss of crystalline nature. Also, an absence of the crystalline peaks of SiW_{12} directs fine dispersion of active species into the support.

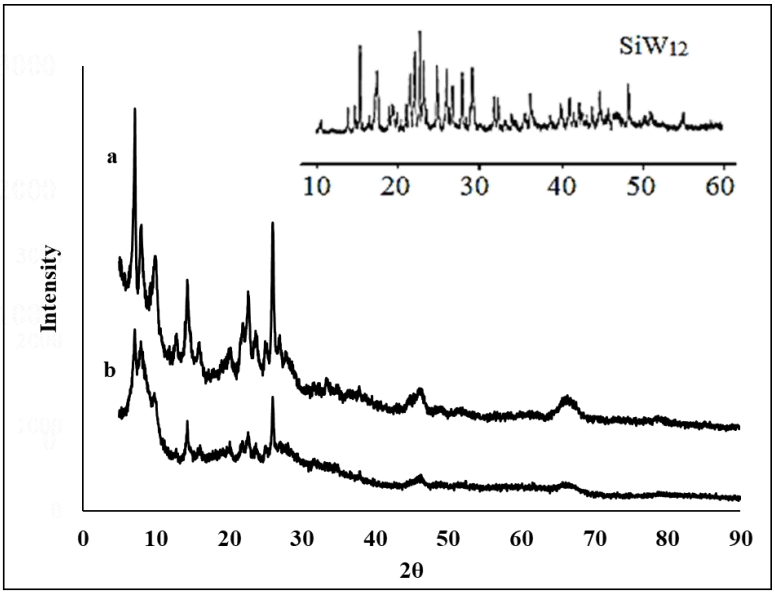

Figure 6 Powder XRD patterns of a) MCM-22, b) SiW_{12}/MCM-22 and SiW_{12} (Inset)

^{29}Si MAS NMR

^{29}Si MAS NMR of MCM-22 and SiW_{12}/MCM-22 are shown in Figure 7. MCM-22 exhibits a distinct peak at -99.34 ppm for the Si nuclei associated with one Al unit and a range of small peaks from –102 to –118 ppm corresponding to other Si (which are not surrounded by Al atoms) [21,22]. Evidently, in the NMR spectra of SiW_{12}/MCM-22, an increase in the intensities of the bunch of peaks was observed accompanied by the change in the chemical shift values. This suggests that there is an increase in the Si nuclei in the framework and these extra sites come from SiW_{12}, suggesting the firm hydrogen bonding of it with the support. Also, an extra peak at 83.79 ppm appears in the spectrum which is due to the Si nuclei present in the Keggin unit. Thus, the above observations confirm the interaction between the SiW_{12} and MCM-22 as well as the unaltered structure of Keggin ion and support.

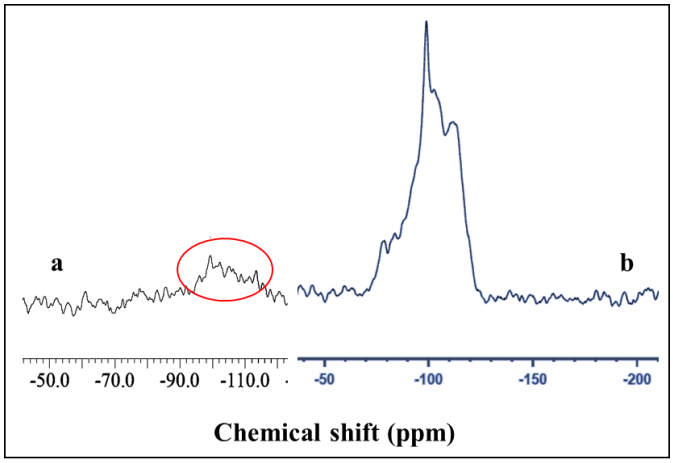

Figure 7 ^{29}Si MASNMR of a) MCM-22 and b) SiW_{12}/MCM-22

TEM

The TEM images of MCM-22 and SiW_{12}/MCM-22 are presented in Figure 8. MCM-22 depicts the formation of a uniform structure by the growth of flaky crystals. The image of a few indistinct pore networks is observed [18]. After impregnation of SiW_{12}, the transparent networks of pores appear to be opaque, signifying a uniform filling inside the pores of MCM-22. This observation was also supported by the XRD patterns, where the absence of crystalline peaks of heteropoly indicates its fine dispersion.

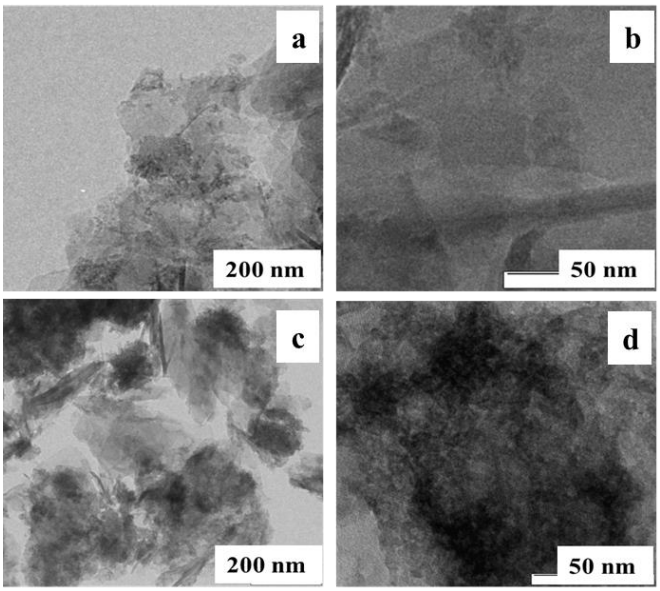

Figure 8 TEM images of a,b) MCM-22 and c,d) SiW_{12}/MCM-22)

In a nutshell, the acidity measurements and BET surface area analysis depict the successful enhancement of acidic character especially the Bronsted acid sites as

well as effective impregnation of SiW_{12} into MCM-22. FT-IR analysis confirms the intact structure of active species and support, whereas the powder XRD, SEM and TEM analysis implies fine and uniform dispersion of SiW_{12} inside the zeolitic support. The ^{29}Si MAS NMR directs the presence of hydrogen bonding between the active species and support. Thus, the above characterization confirms the formation of a novel heterogeneous acid catalyst where the innate properties of individual species are preserved.

Catalytic activity

Leaching test

The leaching of SiW_{12} from the hold of MCM-22 in SiW_{12}/MCM-22 was checked by the method given in General introduction [Page 46]. The absence of heteropoly blue colour indicates no leaching of SiW_{12} from MCM-22 and suggests the presence of chemical interaction between them as well as stability of the catalyst.

a) Esterification of levulinic acid with n-butanol

A detailed optimization study by varying all the reaction parameters such as % loading of SiW_{12}, the mole ratio of levulinic acid to n-butanol, catalyst amount, reaction temperature and time was carried out.

From the catalytic viewpoint, for any new catalyst, it is important to identify the appropriate loading amount of an active species to yield its optimum activity. Experiments with all catalysts (10 to 40% loaded SiW_{12}/MCM-22) were carried out and the obtained results are shown in Figure 9a. Similar to the observations in previous catalysts, here also, the conversion of levulinic acid proceeds with an increase in the amount of SiW_{12}. In 10% loading amount, only 20% conversion with 61% selectivity of butyl levulinate was achieved, whereas the conversion doubled in 40% loading and the selectivity increased to 77%. However, it is interesting to note that in the 30% loading amount, 38% conversion was obtained

which does not differ much from the 40% loading amount. Also, here the highest selectivity of butyl levulinate (94%) was achieved. This observation is quite unusual from the ones obtained in previous catalysts. The selectivity hiked abruptly in 30% loading. Therefore, looking at the conversion as well selectivity, 30% loading of SiW_{12} was found to be optimum and for further experiments, this catalyst was utilized.

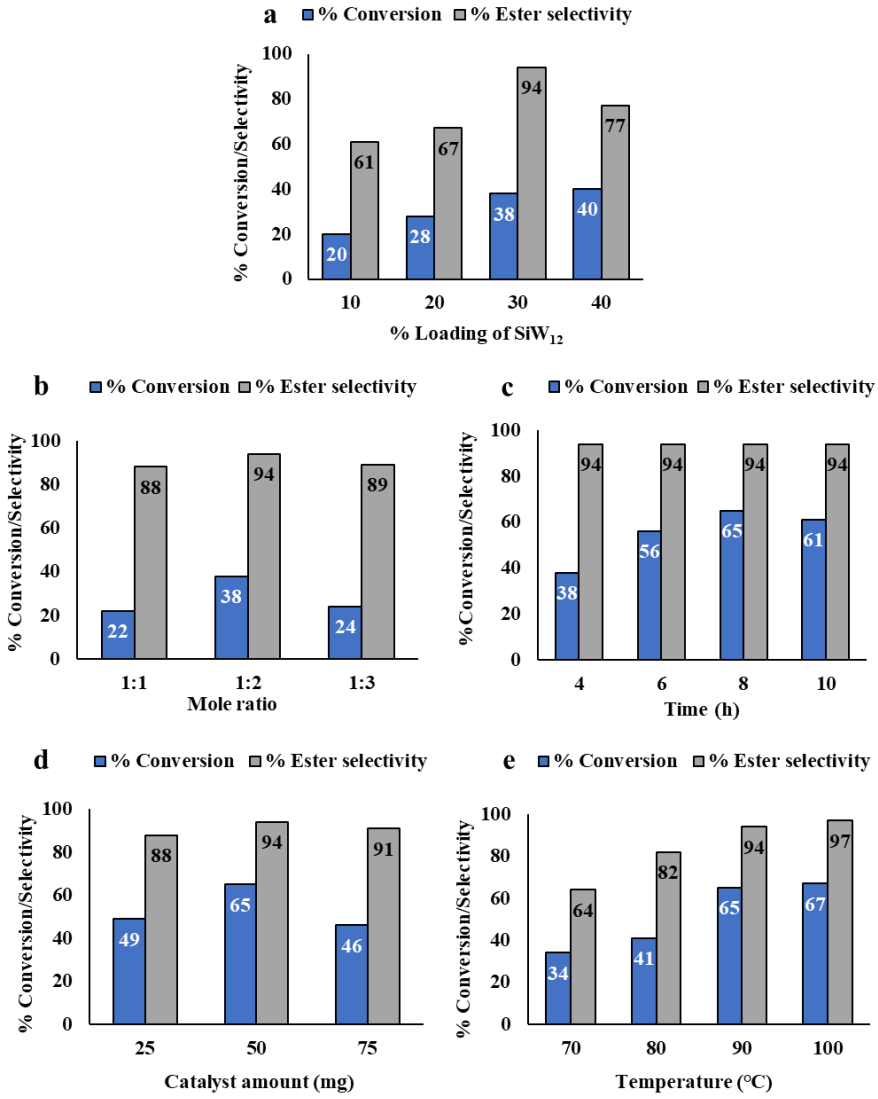

Figure 9 Reaction conditions a) Effect of % loading of SiW_{12}. Mole ratio: 1:2; Catalyst amount: 50 mg; Temperature: 90 °C; Time: 4 h b) Effect of mole ratio. Catalyst amount 50 mg; Temperature 90 °C; Time 4h, c) Effect of time. Mole ratio 1:2; Catalyst amount 50 mg; Temperature 90 °C; d) Effect of catalyst amount. Mole ratio 1:2; Temperature 90 °C; Time 8h, e) Effect of temperature. Mole ratio 1:2; Catalyst amount 50 mg; Time 8h.

The effect of the molar ratio of levulinic acid to alcohol was studied by keeping experiments in 1:1 to 1:3 and the results are plotted in Figure 9b. From 1:1 to 1:2, the conversion of acid increased from 22% to 38%, as anticipated. In equal stoichiometric, the reaction is likely to undergo reverse hydrolysis as some of the water molecules, released as a byproduct may occupy the catalytic sites. Therefore, a little excess alcohol helps in shifting the reaction in a forward direction. Nevertheless, on further increasing the ratio 1:3, conversion drops slightly, due to the dilution of the reaction mixture. Hence, the 1:2 mole ratio is considered appropriate with SiW_{12}/MCM-22.

The next important parameter, reaction time was screened from 4 to 10 h. As observed in Figure 9c, the conversion increases up to 8 h to 65% with no change in the selectivity of ester. But, extending the reaction time to 10 h, a minor decrease in the conversion was observed. This change may be due to the attainment of equilibrium or some of the formed ester molecules undergoes reverse hydrolysis. Thus, 8 h was found to be the optimum reaction time.

The effect of catalyst amount was investigated using 25 to 75 mg catalyst. Figure 9d displays that an increase in catalyst amount has a positive effect on the conversion from 25 mg to 50 mg. maximum conversion, as well as selectivity, was achieved when 50 mg catalyst was used. Before that in a lower catalyst amount, the available catalytic sites were less and in a higher catalyst amount an increase in the reaction mixture viscosity was observed, which lowered the conversion in both cases. So, 50 mg was found to be the required amount.

Figure 9e depicts a significant effect of temperature in reaction. Presumably, a rise in temperature from 70 °C to 100 °C, leads to a gradual increase in the conversion of acid and selectivity towards ester from 34% to 67% and 64% to 97% respectively. At elevated temperature, more collisions between the reactant molecules as well as faster activation of the acid group occurs, which increases the product formation and decreases the chances of the reverse reaction. however, it should be noted that there was no major difference in the results of

the reactions at 90 °C and 100 °C. Thus, looking at the energy consumption factor, 90 °C was optimized as an appropriate reaction temperature.

From the above observations, the optimized reaction conditions for maximum conversion of levulinic acid (65%) and selectivity of ester (94%) are: mole ratio (levulinic acid: n-butanol) 1:2; catalyst amount 50 mg (active amount of SiW_{12} 11.54 mg), temperature 90 °C; time 8h. The TON and TOF were found to be 1621 and 203 h^{-1}, respectively.

b) Esterification of succinic acid with n-butanol

The activity of SiW_{12}/MCM-22 was also studied for the catalytic esterification of succinic acid with n-butanol. Here also, identical to previous chapters, a detailed optimization study was carried out to find the best parameters with SiW_{12}/MCM-22 for obtaining the maximum conversion of acid and selectivity of diester.

Initially, the practicability of the synthesized catalysts for this transformation was checked by keeping the reactions in a series of catalysts i.e., 10 – 40% SiW_{12}/MCM-22 (Figure 10a). With the loading amount, the acid sites responsible for the catalytic activity also increase, which leads to the rise in the conversion of acid. From 10% to 30%, this trend was evident. Also, with the conversion of acid, the diesterification progresses and hence the selectivity increases. However, after a certain amount (30%), in 40% loading, the conversion decreases by 15%. It is assumed that MCM-22 itself possesses some Lewis acid sites as there is the presence of Al atoms in the framework [23,24]. But when the impregnation is done with SiW_{12}, it is supposed that some of these sites are may be occupied and hence the overall availability of sites might become less. Therefore, at higher concentrations, there may be blocking of active sites of support which does not allow the reactants to access the catalytic sites. Thus, considering the maximum conversion as well as selectivity, a 30% loaded catalyst was found to be suitable.

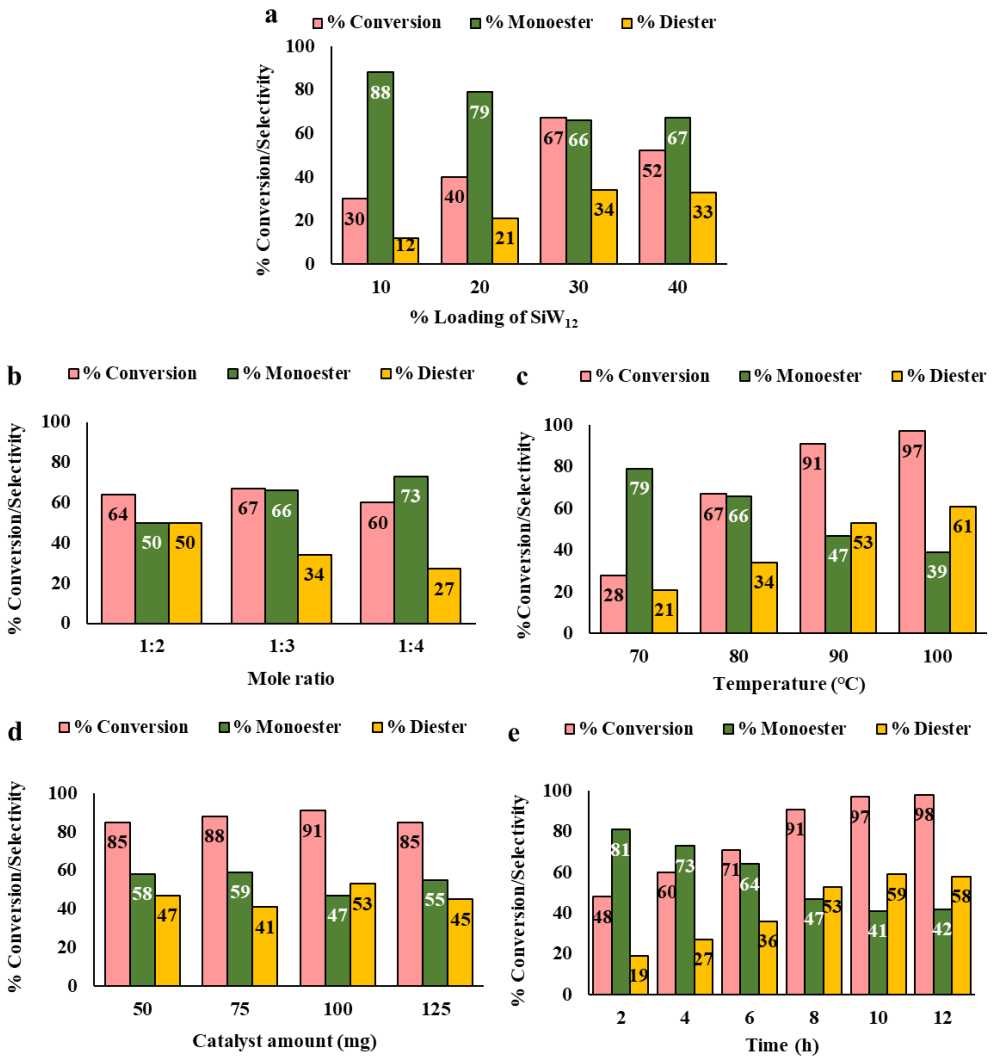

Figure 10 Reaction conditions. a) Effect of % loading of SiW_{12}. Mole ratio 1:3; Catalyst amount 100 mg; Temperature 80 °C; Time 8 h, b) Effect of mole ratio. Catalyst amount 100 mg; Temperature 80°C; Time 8h, c) Effect of temperature. Mole ratio 1:3; Catalyst amount 100 mg; Time 8h d) Effect of catalyst amount. Mole ratio 1:3; Temperature 90°C; Time 8h, e) Effect of time. Mole ratio 1:3; Catalyst amount 100 mg; Temperature 90°C.

A little excess of alcohol is beneficial for an esterification reaction to proceed in a forward direction. Therefore, the mole ratio of acid to alcohol from 1:2 to 1:4 was examined and the results are plotted in Figure 10b. As the mole ratio increases from 1:2 to 1:3, the conversion of succinic acid also upsurges from 63 to 67% with 66% monoester selectivity and 34% diester. However, a further augmentation in alcohol concentration increases the dilution of reaction mass and the conversion rate decreases to 60%. For the initial viability of catalytic

activity, the focus was driven more on acid conversion. Accordingly, a 1:3 ratio was selected.

The reaction temperature is the crucial parameter that has a substantial effect on an esterification process. The esterification reaction of succinic acid was carried out at four different temperatures, 70 to 100 °C (Figure 10c) to understand the trend of product formation. As expected, a remarkable increase in the formation of esters from 28 to 91% was observed in elevated temperatures up to 90 °C. At the same time, the selectivity of the diester increased to 53%. On the contrary, when the reaction was allowed to proceed at 100 °C, a minimal increase in the conversion and selectivity was obtained. Therefore, 90 °C was considered an optimum temperature.

The effect of catalyst amount was studied by keeping experiments in the range of 50 to 125 mg and the results are presented in Figure 10d. Maximum conversion of acid and diester selectivity was achieved when the catalyst amount was raised to 100 mg. The more the availability of catalytic sites, the more the conversion of acid to ester and the better the selectivity of diester was obtained. As there are more acid sites, the monoester is prone to undergo a second esterification reaction and increases the diester formation. Nonetheless, when 125 mg of catalyst was used, a decline in the conversion and selectivity was observed. This decrease may be ascribed to the increase in mass density due to the solvent-free reaction pathway and an insufficient stirring of the reaction mixture because of slurry formation. Consequently, 100 mg of catalyst concentration can be assessed as the required amount [25].

For evaluation of the essential contact time of reactants, the reaction was carried out at different time intervals from 2 h to 12 h (Figure 10e). With progression in reaction time (2 to 10 h), conversion of acid and diester formation increase from 48 to 97% and 19 to 59%, respectively. Along with the catalytic sites, sufficient time interval is vital for the activation of the carbonyl group of acid and also for the second esterification reaction. But, when the reaction was prolonged to 12 h,

no variation in both the conversion and selectivity was observed. Hence, 10 h was optimized as the required reaction time.

The optimized reaction conditions for maximum conversion of succinic acid (97%) and selectivity of diester (59%) are: a mole ratio of acid to alcohol 1:3; catalyst amount 100 mg (active amount of SiW_{12} 23 mg), reaction temperature 90 °C; and reaction time 10 h. The TON and TOF were found to be 1214 and 121 h^{-1} respectively.

c) Acetalization of glycerol with furfural

The efficiency of SiW_{12}/MCM-22 for acetalization of glycerol with furfural was assessed and a detailed optimization study was carried out by varying similar reaction parameters as stated in previous chapters. The conditions for obtaining the maximum conversion of glycerol and selectivity towards dioxane derivative were optimized.

The feasibility of catalysts with different concentrations of SiW_{12} was carried out and the results are tabulated in (Figure 11a). Initially, very low conversion of glycerol, 6 and 12% was observed in 10 and 20% loading, respectively. In 30% loading, the conversion reached 22%, but the selectivity of dioxane decreased slightly and almost similar results were obtained for 40% loading. These low conversion rates in SiW_{12}/MCM-22 can be attributed to the lower acidic nature as well as surface area as compared to that of the nMCM-48 based catalysts. Thus, looking to the maximum conversion of glycerol, here too, the 30% loaded catalyst was optimized and used for further study.

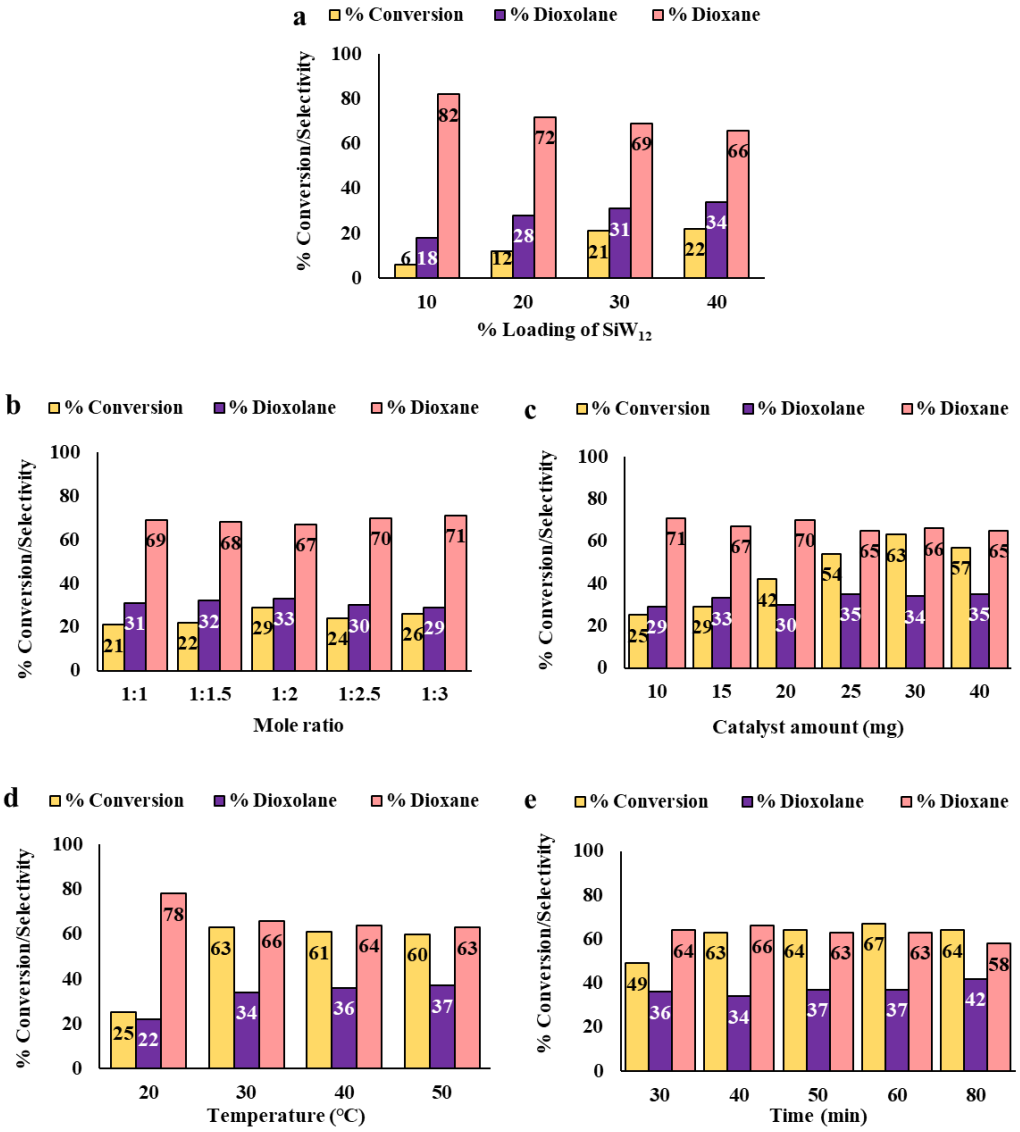

Figure 11 Reaction conditions. a) Effect of % loading of SiW_{12}. Mole ratio 1:1; Catalyst amount 15 mg; Temperature 30 °C; Time 40 min b) Effect of mole ratio. Catalyst amount 15 mg; Temperature 30°C; Time 40 min, c) Effect of catalyst amount. Mole ratio 1:2; Temperature 30°C; Time 40 min, d) Effect of temperature. Mole ratio 1:2; Catalyst amount 30 mg; Time 40 min, e) Effect of time. Mole ratio 1:2; Catalyst amount 30 mg; Temperature 30°C

The mole ratio of both the reactants certainly affects the rate of reaction as well as product formation. Hence the ratio of reactants was studied by carrying out experiments in the range of 1:1 to 1:3 and the obtained results are plotted in Figure 11b. From 1:1 to 1:2, a gradual increase in the conversion of glycerol was observed. Beyond it, the conversion rate decreases steadily, indicating the dilution effect by access furfural which is well explained in the previous chapter.

In the 1:2 mole ratio, even though the dioxane selectivity decreased, it gave maximum conversion of glycerol (29%). Therefore 1:2 ratio was optimized.

Experiments in different catalyst amounts, 10 to 40 mg were assessed and the results are mentioned in Figure 11c. An increase in the catalyst amount leads to the progress of the reaction, regardless of a change in the selectivity of dioxane. The availability of catalytic sites is directly related to the catalyst amount. So, a greater number of furfural molecules gets activated when the catalyst amount was increased. A maximum glycerol conversion of 63% with 66% dioxane selectivity was achieved in 30 mg. However, after that, the conversion slightly decreased to 57% with no major effect on the selectivity of dioxane. Therefore, 30 mg was considered an appropriate catalyst amount.

The influence of temperature was checked in 20 – 50 °C and the obtained findings are shown in Figure 11d. Primarily, at 20 °C, a poor rate of conversion was observed, whereas when the temperature further increase to 30 °C, a sudden rise in the conversion was seen. This may be attributed to the fruitful activation of a greater number of furfural molecules as well as an effective collision between the reactant molecules that promotes the reaction even at just 30 °C temperature. Further rise in temperature does not significantly improve the activity of SiW_{12}/MCM-22. Accordingly, 30 °C temperature was optimized.

The last parameter is to identify the contact time of reactants. The reaction was screened from 30 to 80 mins and the results are displayed in Figure 11e. With time the reaction progressed well giving conversions >60% except in 30 mins. 63% conversion with 66% dioxane selectivity was attained in 40 mins, however, only a 4% rise was observed in subsequent reaction time. Thus, looking at the steady activity of the catalyst, 40 min was considered the required time for the reaction.

The optimized conditions for glycerol acetalization are: mole ratio 1:2, catalyst amount 30 mg (active amount of SiW_{12} 7.0 mg), temperature 30 °C, and time 40

min. at these conditions, a maximum conversion of 63% and 66% selectivity towards 1,3-dioxane, with TON and TOF of 2625 and 3918 h^{-1}, respectively was obtained.

All the products were analysed by gas chromatography and confirmed by their respective standard samples. The gas chromatographs after the reaction in their respective optimized conditions are shown below in Figure 12, Figure 13 and Figure 14.

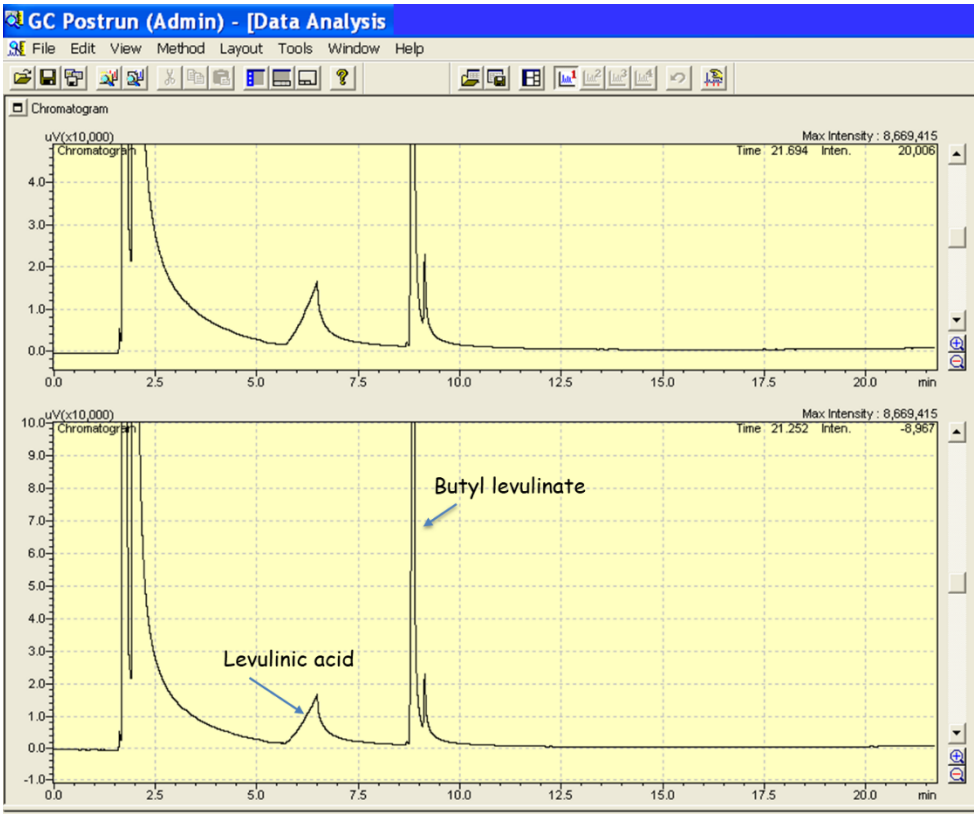

Figure 12 Gas chromatograph of levulinic acid esterification

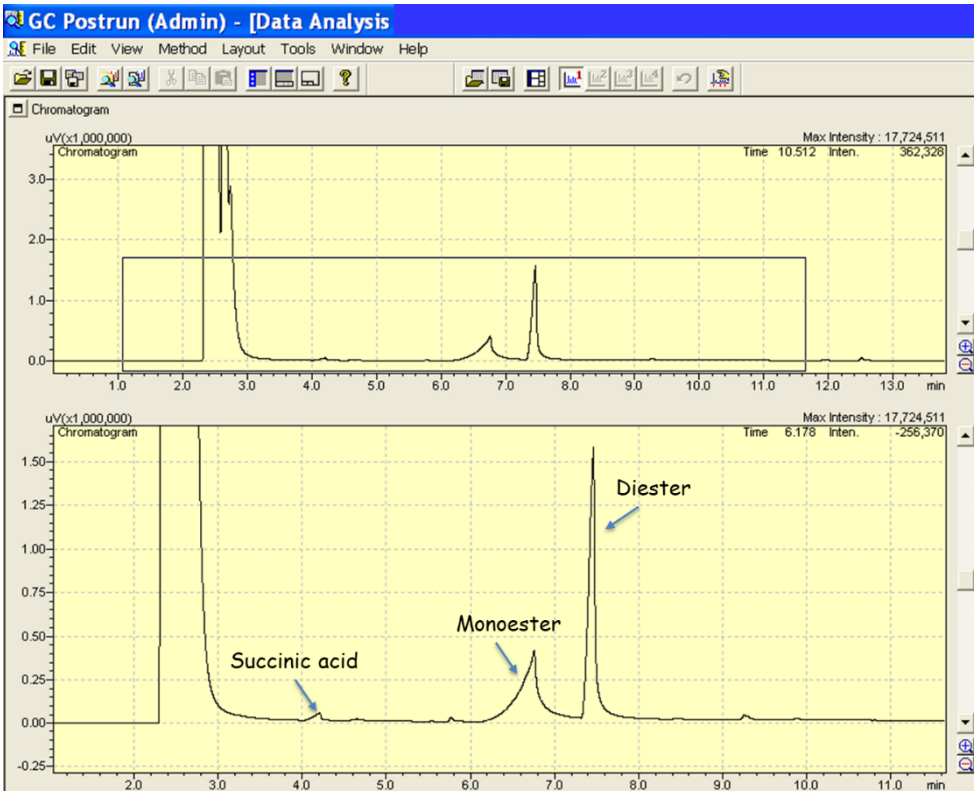

Figure 13 Gas chromatograph of succinic acid esterification

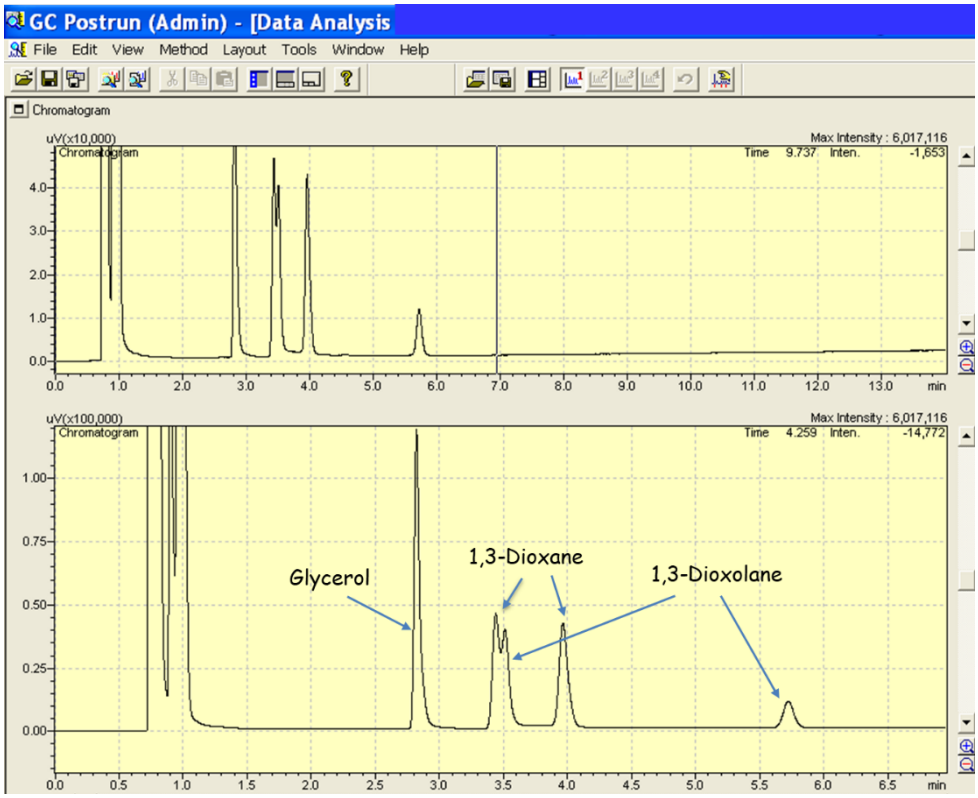

Figure 14 Gas chromatograph of glycerol acetalization

Control experiments

The results of control experiments carried out using MCM-22 and SiW_{12} are depicted in Table 4. It is seen from table that the Bronsted acidity present in SiW12 acts as active species and plays a major role in catalytic activity. Further it also shows that we have successfully synthesized a truly heterogeneous catalyst. It should be noted that the existence of Lewis acidic sites (Al sites) in the support also plays a role in governing the selectivity of products. For instance, lower conversion levulinic acid esterification as compared to bare SiW_{12} as well as directing the selectivity of monoester in succinic acid esterification and the preference of 1,3-dioxane over 1,3-dioxolane in glycerol acetalization. Thus, the change in the conversion as well as selectivity in case of catalyst is due to the synergic effect of MCM-22 and SiW_{12}.

Table 4 Control experiments for SiW_{12}/MCM-22

Materials	% Conversion/%Selectivity of the desired product*		
	[a]Levulinic acid esterification	[b]Succinic acid esterification	[c]Glycerol acetalization
MCM-22	40/83	64/36	29/76
SiW_{12}	98/100	100/98	65/52
SiW_{12}/MCM-22	65/94	97/59	63/66

Reaction conditions mole ratio [a]1:2, [b]1:3, [c]1:2; catalyst amount MCM-22 [a]38.46 mg, [b] 77 mg, [c]23 mg; SiW_{12} [a]11.54 mg, [b]23 mg, [c]7.0 mg; SiW_{12}/MCM-22 [a]50 mg, [b]100 mg, [c]30 mg; temperature [a]90 °C, [b]90 °C, [c]30 °C; time [a]8 h, [b]10 h, [c]40 min.
*Selectivity of [a]Butyl levulinate, [b]Diester (Dibutyl succinate) and [c]1,3-dioxane

Regeneration and recycling studies

The regeneration of the catalyst after the first cycle was carried out by the procedure reported in Part A Chapter 1 and the obtained regenerated catalyst from all transformations, was utilized for consecutive catalytic cycles. The results of the recycling experiments are plotted in Figure 15. Regenerated SiW_{12}/MCM-22 demonstrates reliable catalytic activity for all transformations

up to three cycles and considerable conversion as well selectivity of desired products was obtained for all reactions. However, in the 4th cycle, the activity falls to a noticeable change which may be due to the loss of catalyst amount. Also, some of the product molecules may stick on the catalyst surface which hampers the contact of fresh reactant molecules with it. However, one can use it for more cycles until the complete deactivation of the catalyst. These results validate the sustainability and credibility of the present catalyst for multiple cycles.

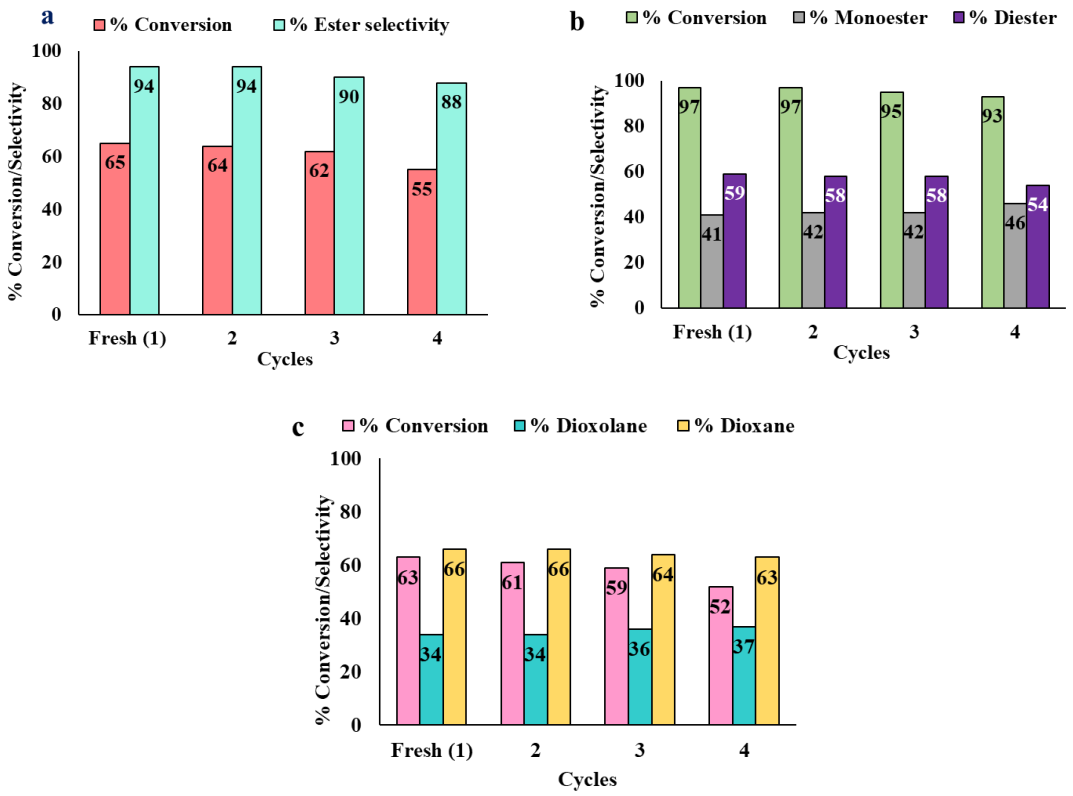

Figure 15 Recycling experiments of a) levulinic acid esterification, b) succinic acid esterification and c) glycerol acetalization

Characterization of regenerated catalyst

Analogous to previous chapters, the regenerated SiW_{12}/MCM-22 was characterized by acidity measurements, BET surface area and FT-IR analysis to confirm its sustainability. The total acidic sites as well as the strength of the regenerated catalyst were found to be similar to that of the fresh one (Table 5). This observation confirms the intact acidic character of the catalyst. The Nitrogen

adsorption-desorption isotherms of regenerates and fresh catalysts (Figure 16a) were found to be identical with almost similar surface area. It indicates the unaltered structure of the catalyst. Besides, in the FT-IR spectra (Figure 16b) of regenerated catalyst, the presence of all characteristic bands stipulates the stability and firm interaction of SiW_{12} with MCM-22. Thus, the nature of the catalyst remains unaffected even after regeneration.

Table 5 Acidity measurements and BET surface area of fresh and regenerated catalyst

Catalysts	Acidic strength (mV)	Total acidic sites (mEq/g)	BET surface area (m^2/g)
Fresh	456	3.7	234
Regenerated	451	3.3	244

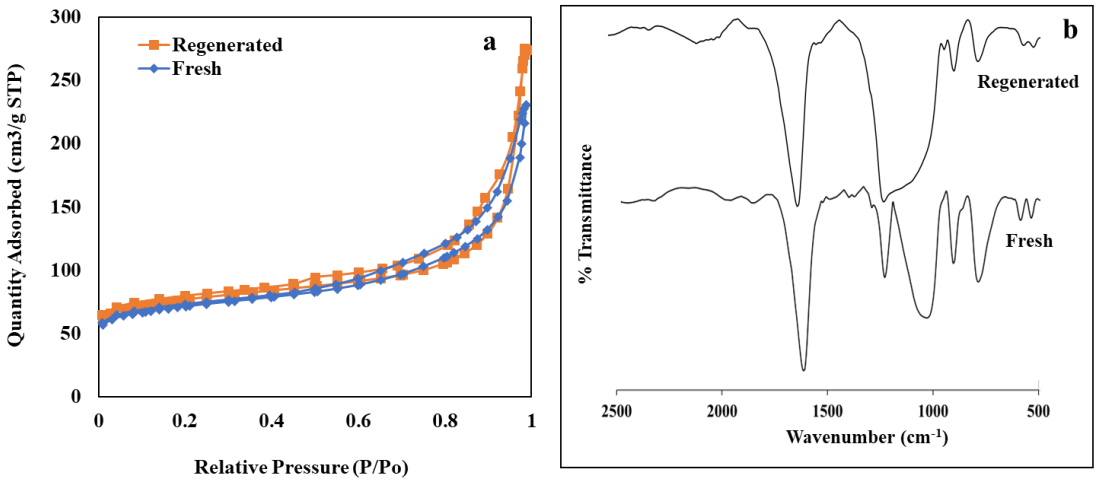

Figure 16 a) Nitrogen adsorption-desorption isotherms and b) FT-IR spectra of regenerated and fresh catalyst

Activity of catalyst for esterification reactions under identical conditions

To study the activity of SiW_{12}/MCM-22 for both esterification reactions, experiment under identical conditions were carried out. The obtained results (Table 6) suggests that SiW_{12}/MCM-22 marginally favours the conversion of levulinic acid (65%) compared to that of succinic acid (60%). However, very low selectivity of desired diester was observed. This indicates that here also, the

activity of catalyst is more for esterification of keto acid, as compared to diacid and the explanation remains the same as given in Part A Chapter 1.

Table 6 Esterification reactions under identical conditions

Conditions / Reactions	In optimized conditions of levulinic acid esterification*	
	% Conversion of acid	% Selectivity of desired ester
Levulinic acid esterification	65	94
Succinic acid esterification	60	46 (Diester)

*Reaction conditions mole ratio 1:2; catalyst amount 50 mg; temperature 90 °C; time 8 h

Kinetic study: Determination of activation energy

The activation energy for esterification, as well as acetalization reactions using SiW_{12}/MCM-22, was determined by studying the reaction at different temperatures and time intervals.

a) Activation energy for esterification of levulinic acid with n-butanol

The obtained results of experiments for esterification of levulinic acid in a 1:2 mole ratio with n-butanol at different time intervals (6, 8 and 10 h at 90 °C) were considered to plot a graph of 1/(a-x) versus time (Figure 17). The plot depicts a linear relationship of reaction with respect to time and validates its second-order dependence.

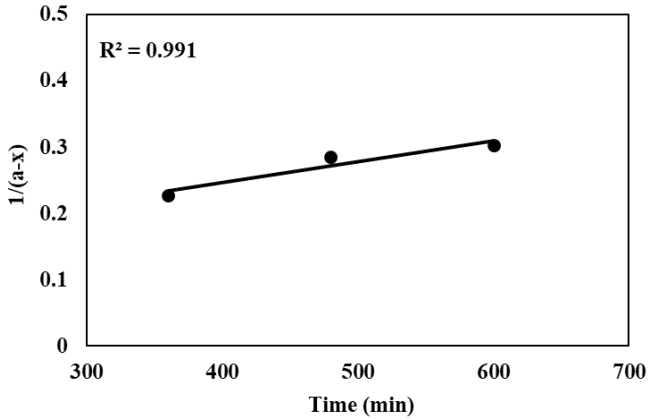

Figure 17 Plot of 1/(a-x) Vs Time for levulinic acid esterification

The rate constants at each temperature, 343, 353, 363 and 373 K (in different time intervals) were calculated and tabulated in Table 7. As observed in the previous chapter, here also the temperature as a positive effect on the rate constant. From these values, a graph of ln *k* Vs 1/T was plotted (Figure 18) from the slope of the graph, the activation energy was found to be 36 kJ/mol using the Arrhenius equation.

Table 7 Rate constants (*k* M^{-1} min^{-1}) and activation energy (Ea)

Temperature (K)	Rate constant *k* (M^{-1} min^{-1})	Activation energy Ea (kJ/mol)
343	3.0×10^{-4}	36
353	4.0×10^{-4}	
363	6.0×10^{-4}	
373	8.0×10^{-4}	

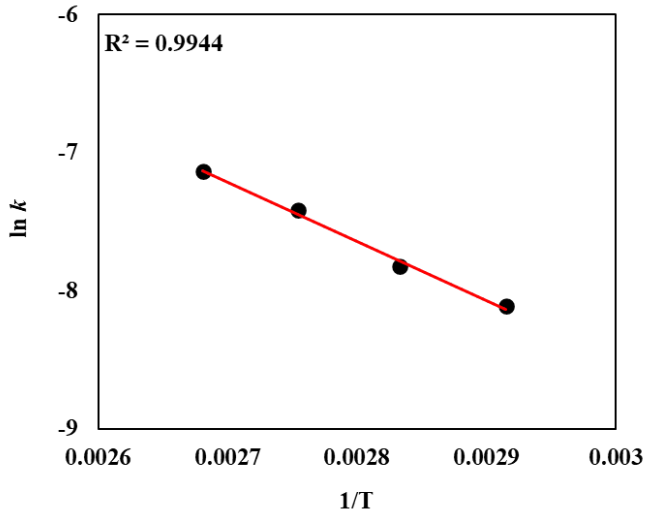

Figure 18 Plot of ln *k* Vs 1/T for levulinic acid esterification

b) Activation energy for esterification of succinic acid with n-butanol

Similar to previous studies, from the obtained results of kinetic experiments for the esterification of succinic acid and n-butanol using SiW_{12}/MCM-22 in 1:3 molar ratio for different time intervals (6, 8 and 10 h) at 90 °C, the graph of 1/(a-x) Vs Time was plotted (Figure 19). The graph shows a linear plot, suggesting the second-order dependence of the reaction.

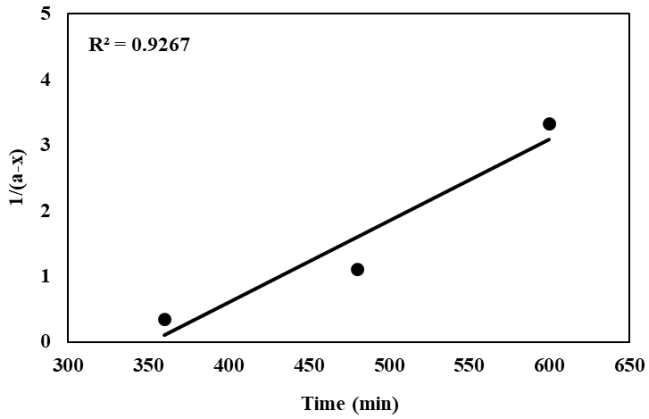

Figure 19 Plot of 1/(a-x) Vs Time for succinic acid esterification

To determine the rate constants at different temperatures (353 to 383 K), the reactions were carried out at different time intervals and the results are shown in Table 8. From the above results, the graph of ln *k* versus 1/T was plotted

(Figure 20) and from the slope of the graph, by using the Arrhenius equation, the activation energy was calculated and found to be 68 kJ/mol.

Table 8 Rate constants (k M^{-1} min^{-1}) and activation energy (Ea)

Temperature (K)	Rate constant k (M^{-1} min^{-1})	Activation energy Ea (kJ/mol)
353	5.52 x 10^{-3}	68
363	1.12 x 10^{-3}	
373	1.49 x 10^{-3}	
383	3.70 x 10^{-3}	

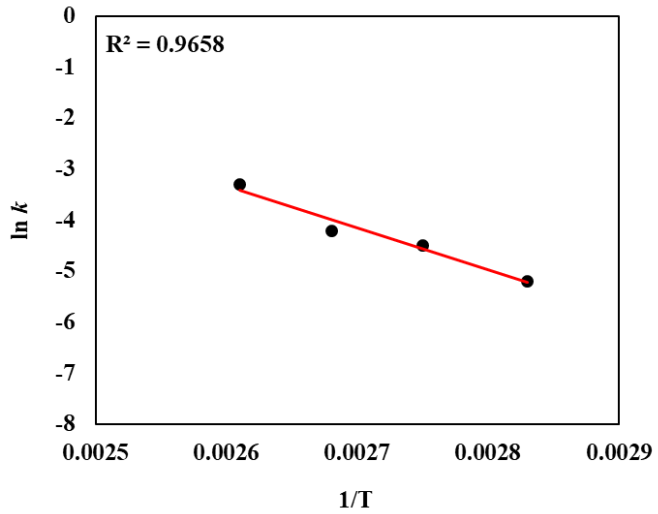

Figure 20 plot of ln k Vs 1/T for succinic acid esterification

c) Activation energy for acetalization of glycerol with furfural

A graph of 1/(a-x) Vs Time was plotted (Figure 21) from the results obtained by carrying out the acetalization reaction of glycerol with furfural using SiW_{12}/MCM-22 in 1:2 mole ratio at 30 °C in different intervals. As observed from the figure, the graph shows a linear relationship with respect to time, hence it can be stated that reaction follows second-order dependence.

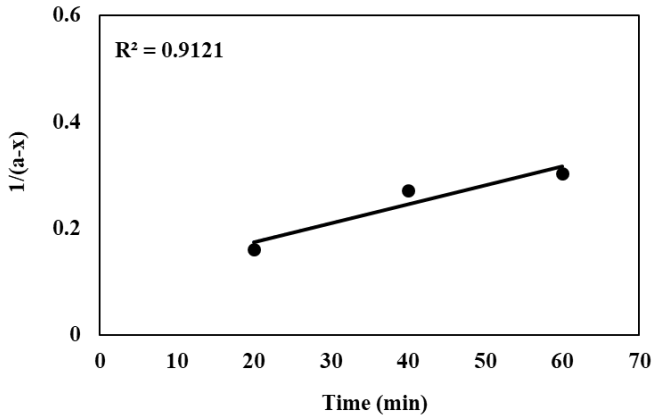

Figure 21 Plot of 1/(a-x) Vs Time for glycerol acetalization

In order to determine the rate constants at different temperatures (293, 303, 313 and 323 K) (Table 9), the reactions were carried out at different time intervals and from the results, the graph of ln *k* Vs 1/T was plotted (Figure 22). The activation energy was calculated from the slope of the graph using the Arrhenius equation and found to be 48 kJ/mol.

Table 9 Rate constants (*k* M^{-1} min^{-1}) and activation energy (Ea)

Temperature (K)	Rate constant *k* (M^{-1} min^{-1})	Activation energy Ea (kJ/mol)
293	1.12×10^{-3}	48
303	3.54×10^{-3}	
313	4.76×10^{-3}	
323	7.8×10^{-3}	

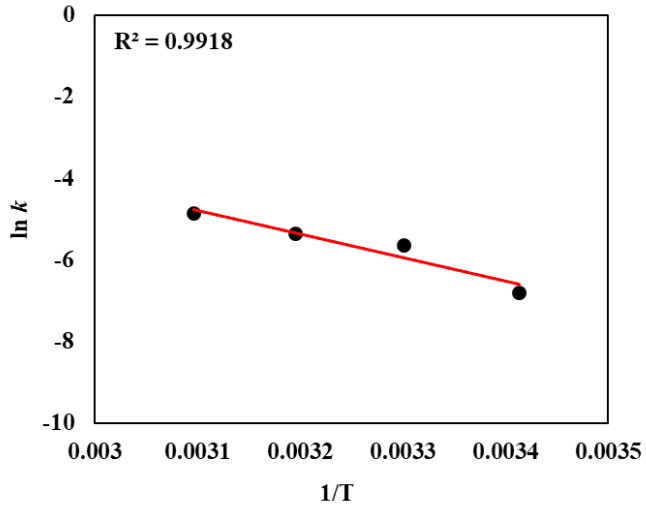

Figure 22 Plot of ln *k* Vs 1/T for glycerol acetalization

The activation energy for all three reactions using SiW_{12}/MCM-22 was found to be exceeding 25 kJ/mol, which indicated that all the reactions are truly governed by a chemical step and none of them follows a diffusion regime. This observation was also evident in the kinetic study with previous catalysts.

Also, the present catalyst at its maximum efficiency is capable of lowering the activation energy for esterification of levulinic acid more as compared to that for esterification of succinic acid. This observed trend is similar to that obtained for nMCM-48 based catalysts where more energy is required for converting monocarboxylic acid to ester than a dicarboxylic acid.

Plausible mechanism

a) Esterification of levulinic acid with n-butanol

The plausible reaction mechanism for the acid-catalyzed esterification of levulinic acid over SiW_{12}/MCM-22 is shown in Figure 23. Primarily, the levulinic acid gets attracted and adsorbed on the support, MCM-22 and the presence of Bronsted acid sites (from SiW_{12}) as well as some of the weak Lewis acid sites (from Al of MCM-22), activates the carbonyl carbon of the carboxylic acid group, thus generating a carbocation. It is important to note that here in SiW_{12}/MCM-22, there is the presence of both Bronsted and Lewis acid sites and so the acidic

sites, in general, are designated as 'A'. During the impregnation of SiW_{12}, it is assumed that only some of the Al sites present in MCM-22 get occupied and the remaining sites may assist to work as the weak acid sites in the activation of acid. In no time, after the formation of the carbocation intermediate, the nucleophilic attack of the hydroxyl group of alcohol occurs and forms an oxonium intermediate. The negative charges of deprotonated SiW_{12} stabilize the oxonium intermediate. It then loses a molecule of water forming the desired ester product and regenerating the acid catalyst. This mechanism supports the results obtained in the optimization study as well as the kinetic study which suggests that compared to the nMCM-48 based catalyst, here the rate of reaction is slightly lower. This difference can be attributed to the lower surface of MCM-22, however, it manages well for the transport of reactant molecules because of its two types of pore systems. Undoubtedly, the Bronsted acidity of SiW_{12} has a major role to play in the catalytic activity but it cannot be ignored that the pore system of MCM-22 avoids the mass transfer problems and provides easy access to reactant molecules towards the active sites.

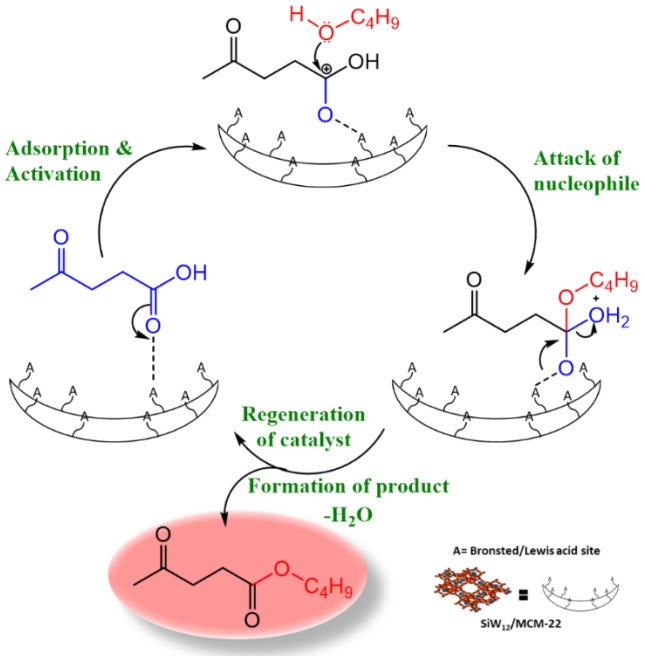

Figure 23 Plausible mechanism of esterification of levulinic acid with n-butanol over SiW_{12}/MCM-22

b) Esterification of succinic acid with n-butanol

The plausible mechanism for esterification of succinic acid with n-butanol is shown in Figure 24. As mentioned in the above mechanism, here we assume that both Bronsted as well as the Lewis acidity contributes to the catalytic activity. However, Bronsted acidity is chiefly responsible for diester formation. The formation of both the esters, mono and diester, follows the same reaction mechanism depending on the competitive adsorption of alcohol and the acidity of the catalyst. Initially, the carboxylic acid gets adsorbed and activated by the Bronsted/Lewis acid sites ('A') present in the catalyst and forms a protonated intermediate (electrophile/carbocation). The nucleophilic alcohol attacks the activated carbonyl carbon, forming a tetrahedral intermediate. At the expense of a water molecule, the intermediate forms monoester (monobutyl succinate), followed by its desorption. The monoester goes through the same pathway to give diester (dibutyl succinate) [26]. The strong acid sites, i.e., Bronsted acid sites are the driving force in activating the acid group of monoester, as after the first esterification it is expected that the pKa value of monocarboxylic acid will be lower as compared to that of dicarboxylic acid. Therefore, to achieve higher selectivity of diester, a little push by the factors such as strength and number of acid sites, elevated temperature, and prolonged time works as a boon.

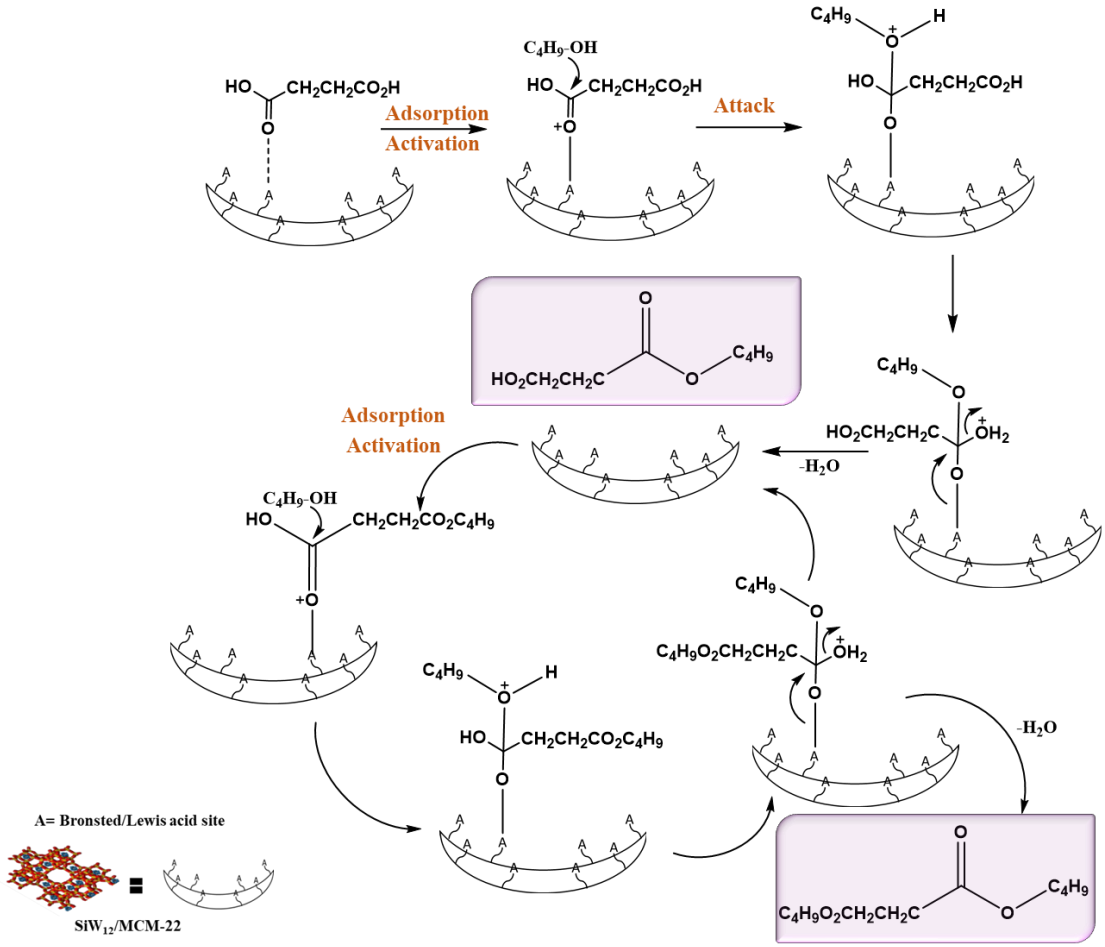

Figure 24 Plausible mechanism of esterification of succinic acid with n-butanol over SiW_{12}/MCM-22

c) Acetalization of glycerol with furfural

The mechanism for the acid-catalyzed acetalization reaction of glycerol with furfural is shown in Figure 25. Firstly, the adsorption of furfural and activation of its carbonyl carbon occurs on the active catalytic site. The carbonyl carbon of the aldehyde group orients itself to Bronsted/Lewis acid sites, and the formation of carbocation/electrophile occurs. Following this, the primary hydroxyl group which is more nucleophilic than the secondary one, attacks the electrophilic site forming a tetrahedral intermediate. On the competitive terms, and alignment of the intermediate, either the 2nd primary or the secondary hydroxyl group attacks the electrophilic center, generated in the intermediate, to form cyclic acetals of glycerol. Looking to the selectivity obtained in the optimized condition, here,

the attack by 2nd primary hydroxyl group is predominant over the secondary hydroxyl group. Therefore, higher selectivity towards 1,3-dioxane was achieved. Both the acetals are interconvertible, however, the thermodynamically stable product, 1,3-dioxane is favoured by the catalyst which may be due to its specific orientation inside the porous channels of support and we assume that after the reaction, the catalyst also plays role in stabilizing the dioxane derivative which avoids its interconversion into dioxolane.

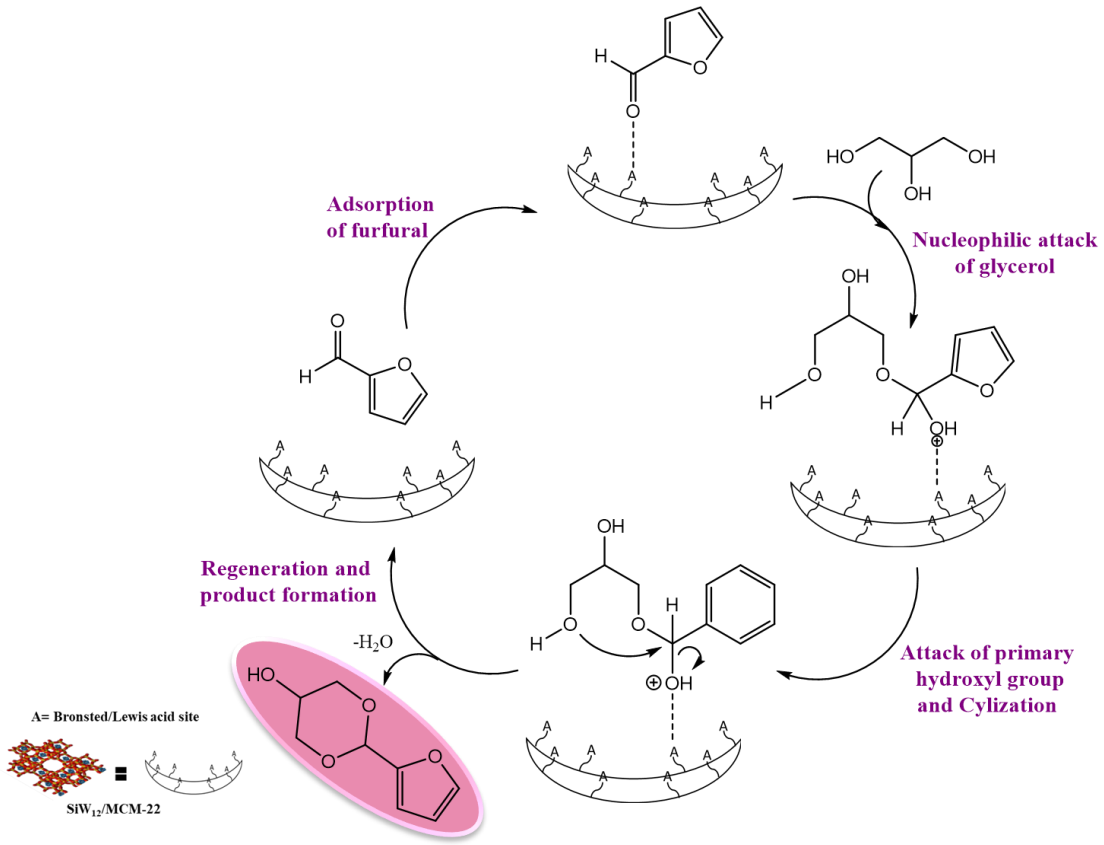

Figure 25 Plausible mechanism of acetalization of glycerol with furfural over SiW_{12}/MCM-22

CONCLUSION

- Successful synthesis and detailed characterization of SiW_{12} modified MCM-22 was carried out. The acidity measurement by potentiometric titration proves the acidic nature of the catalyst, while the BET surface area analysis and FT-IR depict that SiW_{12} is well impregnated onto the MCM-22 support. The interaction of SiW_{12} with the MCM-22 was established by ^{29}Si MAS NMR analysis. TEM and Powder XRD analysis confirm the intact morphology and well dispersion of SiW_{12}.

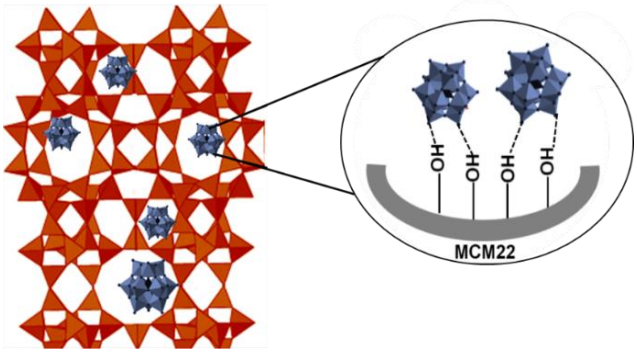

- The synergistic contributions of SiW_{12} and MCM-22 brings out commendable activity for the synthesis of fuel additives.
- The conversion/selectivity of desired products were found to be 65/94% for levulinic acid esterification, 97/59% for succinic acid esterification and 63/66% for glycerol acetalization, with an excellent TONs and TOFs in the range of 1214-2625 and 121-3918 h^{-1}, respectively.
- The activation energy for levulinic acid esterification (36 kJ/mol) was found to be lowest as compared to that of glycerol acetalization (48 kJ/mol) and succinic acid esterification (68 kJ/mol).

REFERENCES

1. M. Kollár, R. M. Mihályi, G. Pál-Borbély, and J. Valyon, Microporous Mesoporous Mater 99, 37 (2007).

2. B. Zhang, Z. Wang, P. Ji, Y. Liu, H. Sun, W. Yang, and P. Wu, Microporous Mesoporous Mater 179, 63 (2013).

3. C. S. Carriço, F. T. Cruz, M. B. Santos, H. O. Pastore, H. M. C. Andrade, and A. J. S. Mascarenhas, Microporous Mesoporous Mater 181, 74 (2013).

4. Y.-Y. Wang, H.-H. Wang, T.-L. Chuang, B.-H. Chen, and D.-J. Lee, Energy Procedia 61, 933 (2014).

5. P. Sahu, S. Eniyarppu, M. Ahmed, D. Sharma, and A. Sakthivel, J Porous Mater 25, 999 (2018).

6. B. A. Abdulkadir, A. Ramli, L. J. Wei, and Y. Uemura, J Jpn Inst Energy 97, 191 (2018).

7. D. Xu, H. Lv, and B. Liu, Front Chem 6, 550 (2018).

8. M. Nawab, S. Barot, and R. Bandyopadhyay, New J. Chem. 43, 4406 (2019).

9. L. Liu, R. Arenal, D. M. Meira, and A. Corma, ChemComm 55, 1607 (2019).

10. A. Galadima and O. Muraza, Catal Surv from Asia 23, 149 (2019).

11. Z. Chen, D. Situ, J. Zheng, Z. Cheng, Z. Wang, and S. Zuo, Catalysts 9, 902 (2019).

12. A. Wojtaszek-Gurdak, V. Calvino-Casilda, A. Grzesinska, R. Martin-Aranda, and M. Ziolek, Microporous Mesoporous Mater 280, 288 (2019).

13. Y. Wang, Y. Gao, S. Xie, S. Liu, F. Chen, W. Xin, X. Zhu, X. Li, N. Jiang, and L. Xu, Catal Today 316, 71 (2018).

14. R. Thakkar and R. Bandyopadhyay, in Advances in Spectroscopy: Molecules to Materials (Springer, 2019), pp. 301–310.

15. I. Julian, J. L. Hueso, N. Lara, A. Solé-Daurá, J. M. Poblet, S. G. Mitchell, R. Mallada, and J. Santamaría, Catal Sci Technol 9, 5927 (2019).

16. M. Thommes, K. Kaneko, A. v. Neimark, J. P. Olivier, F. Rodriguez-Reinoso, J. Rouquerol, and K. S. W. Sing, Pure Appl. Chem. 87, 1051 (2015).

17. C. Delitala, M. D. Alba, A. I. Becerro, D. Delpiano, D. Meloni, E. Musu, and I. Ferino, Microporous Mesoporous Mater 118, 1 (2009).

18. Y. Cheng, X. Y. Su, and M. Lu, Adv Mat Res 197–198, 1587 (2011).

19. P. Kapse, IAETSD J Adv Res Appl Sci 5, 192 (2018).

20. E. Xing, Y. Shi, W. Xie, F. Zhang, X. Mu, and X. Shu, RSC Adv 5, 8514 (2015).

21. W. Kolodziejski, C. Zicovich-Wilson, C. Corell, J. Perez-Pariente, and A. Corma, J Phys Chem 99, 7002 (1995).

22. A. L. Santos Marques, J. L. Fontes Monteiro, and H. O. Pastore, Microporous Mesoporous Mater 32, 131 (1999).

23. D. Ma, X. Han, S. Xie, X. Bao, H. Hu, and S. C. F. Au-Yeung, Chem Eur J 8, 162 (2002).

24. M. Bevilacqua, D. Meloni, F. Sini, R. Monaci, T. Montanari, and G. Busca, J Phys Chem C 112, 9023 (2008).

25. C. Xiros, M. Janssen, R. Byström, B. T. Børresen, D. Cannella, H. Jørgensen, R. Koppram, C. Larsson, L. Olsson, A.-M. Tillman, and S. Wännström, Biofuel Bioprod and Biorefin 11, 15 (2017).

26. C. Jing, L. Jinhua, D. Zhongxie, W. Yuehua, L. Zhen, J. Min, and R. Xiaoqian, Química Nova 41, 613 (2018).